Energy Conversion and Management 180 (2019) 1185–1195

Contents lists available at ScienceDirect

Energy Conversion and Management

journal homepage: www.elsevier.com/locate/enconman

Optimization of fins fitted phase change material equipped solar photovoltaic under various working circumstances

Sourav Khanna[a,*], Sanjeev Newar[b], Vashi Sharma[c], K.S. Reddy[d], Tapas K. Mallick[a,*]

[a] Environment and Sustainability Institute, Penryn Campus, University of Exeter, Cornwall TR10 9FE, United Kingdom
[b] Department of Industrial and Management Engineering, Indian Institute of Technology Kanpur, Kanpur 208016, India
[c] Department of Mechanical Engineering, Indian Institute of Technology Kanpur, Kanpur 208016, India
[d] Heat Transfer and Thermal Power Laboratory, Department of Mechanical Engineering, Indian Institute of Technology Madras, Chennai 600 036, India

ARTICLE INFO

Keywords:
Phase change material
Photovoltaic
Thermal management
Power enhancement
Fins

ABSTRACT

The present work aims at the optimization of fins fitted phase change material equipped photovoltaic system under different working circumstances for proper power enhancement. Setup has been modelled and the best deepness of fins fitted phase change material enclosure has been computed for a range of daily collective solar flux at photovoltaic panel surface, wind pace, wind azimuth, surroundings temperature, melting point, successive fins distance, fins deepness and fins width in order to analyse the influence of working circumstances. It is shown that the change in wind pace from 0.2 m/s to 6 m/s results in reduction of best deepness of phase change material enclosure from 5.2 cm to 3.7 cm, 5.6 cm to 4.0 cm, 5.8 cm to 4.2 cm, 5.9 cm to 4.3 cm and 5.9 cm to 4.3 cm for successive fins distance of 1 m, 1/2 m, 1/3 m, 1/4 m and 1/5 m respectively for daily collective solar flux at photovoltaic panel as 5000Wh/m^2. The change in wind azimuth from 0° to 75° results in increment in the best deepness of enclosure from 3.9 cm to 4.8 cm, 4.3 cm to 5.2 cm, 4.5 cm to 5.4 cm, 4.6 cm to 5.5 cm and 4.6 cm to 5.5 cm for respective fins distances. The power production is increased from 125 W/m^2 to 137 W/m^2, 140 W/m^2, 142 W/m^2, 143 W/m^2 and 143 W/m^2 with fins width of 0 mm, 0.5 mm, 1 mm, 2 mm and 4 mm respectively.

1. Introduction

Heat generation in photovoltaic (PV) hampers power generation due to the lowered efficiency caused by temperature raised. Different mechanisms to keep PV temperature within acceptable range are presented in the literature. Cooling by phase change material (PCM) being one of them has been reported by researchers on both theory and experimental aspects. The summary of the same is discussed in the following subsections.

1.1. Works involving experiments

Polyethylene Glycol PCM has been used for the city of Tehran (Iran) to study the PV behaviour by Baygi and Sadrameli [1] and found to have successfully brought down the temperature of the PV by 15 °C from the case of 60 °C when no PCM is used. Huang et al. [2] have used a dummy PV with PCM – paraffin wax 25 to cool down artificially heated plate to establish that the temperature elevation can be controlled upto the extent of 36 °C from 62 °C. It can further be improved by an additional cooling by fitting fins immersed in the PCM [3]. Distinct environmental conditions of Vehari and Dublin have been studied vis a vis performance of PV supported by calcium chloride hexahydrate [4]. The maximum cooling achieved for the two places has been recorded from 63 °C to 41.5 °C and 49 °C to 39 °C respectively. Indartono et al. [5] considered Indonesian climate for two different PV-PCM systems. One has been the stand-supported PV with PCM- vaselinum flavum with observed cooling from 44.8 °C to 42.2 °C. The system has been compared with other roof-stick PV with same PCM which exhibited cooling from 60 °C to 54.3 °C. Several distinct PCMs have been studied by Hasan et al. [6] and the maximum cooling yielded has been reported from 57 °C to 39 °C with calcium chloride hexahydrate and capric–palmitic acid. PCM's melting kinetics has been studied by Kamkari and Groulx [7] with heating of PCM- lauric acid from lower side. It was established that rate of melting of PCM is higher when the enclosure is kept flat rather than erect or inclined. Sharma et al. [8] have studied non-symmetric parabolic concentrator PV (compound type) fitted with PCM- paraffin wax 42 and achieved cooling from 60 °C to 51 °C. A novel type of PCM (mixed with nano-particles) has been

* Corresponding authors.
E-mail addresses: s.khanna@exeter.ac.uk (S. Khanna), t.k.mallick@exeter.ac.uk (T.K. Mallick).

https://doi.org/10.1016/j.enconman.2018.10.105
Received 27 May 2018; Received in revised form 30 October 2018; Accepted 31 October 2018
Available online 06 December 2018
0196-8904/ © 2018 The Author(s). Published by Elsevier Ltd. This is an open access article under the CC BY license (http://creativecommons.org/licenses/BY/4.0/).

Nomenclature

C	Kozeny-Carman (permeability) constant (kg/m^{3}s)
C_p	specific heat (J/kgK)
D	heat of fusion's distribution function during change of phase
d_e	deepness of PCM enclosure (m)
d_f	deepness of fin (m)
d_{sf}	distance between successive fins (m)
F	shape factor
F_a	volume force in PCM (N/m^3)
g	acceleration due to gravity (m/s^2)
h	convection heat transfer (W/m^{2}K)
H_f	heat of fusion (J/kg)
k	conductivity of material (W/mK)
l	part of total PCM mass in liquefied form
L	enclosure length (m)
Nu	Nusselt number
p	pressure (Pa)
Ra	Rayleigh number
S	solar energy density at PV (W/m^2)
s_w	wind pace (m/s)
t	time (s); thickness (m)
T_m	phase change material's melting temperature (K)
$T_{P,s}$	solidus temperature for PCM (K)
$T_{P,l}$	liquidus temperature (K)
t_{si}	silicon thickness (m)
u_x	phase change material's speed along length (m/s)
u_y	phase change material's speed along deepness (m/s)
w_f	width of fin (m)

Greek Letters

β	inclination of the system (°)
β_c	temperature coefficient (/K)
γ_w	wind azimuth (°)
ε	emissivity for reradiation
μ	viscosity of phase change material (kg/ms)
ρ	density (kg/m^3)
$(\tau\alpha)_c$	combined glass transmittance and PV absorptance
υ	viscosity (m^2/s)

Subscripts

al	aluminium
c	critical
f	front
gl	glass
gr	ground
l	liquid state
P	PCM
r	rear
s	solid state
si	silicon
sk	sky
STC	standard test conditions
te	tedlar
x	along length
y	along deepness

Abbreviation

EVA	ethylene vinyl acetate
CPV	concentrating photovoltaic
CPV-T	concentrating photovoltaic thermal
PV	photovoltaic
PCM	phase change material
PVT	photovoltaic-thermal

considered for the study by Sharma et al. [9] fitted with micro fins. The arrangement achieved cooling of PV from 72 °C to 59 °C. Multiple PCM heat sink configuration for the thermal management has been analysed by Siyabi et al. [10]. The thermal management of concentrating photovoltaic (CPV) using 3 layered stacked heat sink is also analysed [11]. Preet et al. [12] have performed experiments for the climate of Gurdaspur (India) with photovoltaic-thermal (PVT) collector. Also, the system has been equipped with PCM- paraffin wax 30 and measurements are recorded. Latter case is found to have experienced cooling from 80 °C to 55 °C. A PCM made up of different compounds has been used by Browne et al. [13] by making sure they do not interact chemically. Palmitic fatty acids and capric acids are mixed together for the purpose. It is found that the PCM cooled PVT can achieve a thermal efficiency of 20–25% [14]. It is also reported that the novel PCM system can raise the temperature of water by 5.5 °C as compared to PVT system [15]. Su et al. [16] have worked on the concentrating tracking systems. Concentrating Photovoltaic- Thermal (CPV-T) tracking system is studied. The experiments with PCM (paraffin wax) enabled CPV-T is also performed which witnessed a significant 10% improvement in power efficiency for Macau.

1.2. Theoretical works

Brano et al. [17] have handled space-time dimensions separately. For space, the central difference model has been applied. For time, forward difference model has been used. The comparison of the theoretical and observed values suggests a fair accuracy of the models with deflection lying within −5°C to +3 °C when PCM- paraffin wax 27 is used [18]. PCM permeated graphite has been investigated by Atkin and Farid [19] for the performance enhancement and 7% increase in power production has been reported. Kibria et al. [20] worked on PCM's enthalpy modelling using implicit scheme. Three PCMs – paraffin wax 20, 25 and 28 have been considered for the study. It is reported that when paraffin wax 20 gets fully liquefied, paraffin 25 and 28 are only liquified by the fractions of 0.80 and 0.65 respectively. Biwole et al. [21] worked on capturing PCM's change of phase using appropriate modelling so that the possibilities of non-convergence in this error-prone zone can be ruled out. It is also reported that the fins in the PCM enclosure can reduce the standard deviation of the front plate temperature [22] and the increment in the tilt of enclosure can increase the melting speed [23]. Kant et al. [24] compared models of conduction alone and conduction-convection for the PCM in UP (India) which yielded cooling from 60 °C to 58.5 °C and 60 °C to 55 °C respectively for PCM- paraffin 35. Best melting point as 25 °C for the PCM and impact of orientation angle for Incheon has been reported by Park et al. [25]. Su et al. [26] found out the optimum PCM melting point for PVT corresponding to highest energy output. Khanna et al. [27] reported the influence of climates on the utility of phase change material and finned phase change material [28] for PV. It is found that the climates with lesser variations in ambient temperature, less windy climates and hot climates are more suitable for the PCM integration with PV. Khanna et al. [29] have computed the best dimensions of fins in Finned-PV-PCM system. It is found that the fins with deepness same as that of PCM enclosure, spacing of 25 cm and width of 2 mm are the best for PV cooling. Khanna et al. [30] have worked on the optimization of PCM quantity in PV-PCM system for various solar radiation levels. It is found that 3.9 cm is the optimum depth of PCM container for PV cooling for 5 kWh/m^2/day of incident solar radiation. Khanna et al. [31] reported the behaviour of

phase change material enabled PV as function of system's slope and established that non-zero slopes are always better than zero-slope. Khanna et al. [32] have analyzed the electrical performances of 4kWp PV and PV-PCM systems for South West UK climate. It is found that the daily electrical output can be increased from 17.7kWh/day to 18.9kWh/day using PCM. Khanna et al. [33] have analysed different types of solar cells and analysed the influence of working conditions on their electrical performances. Various heat-exchangers rejecting heat to PCM are studied by Emam and Ahmed [34] and the one having parallel channels are found ahead in performance than that with chained arrangement. Huang et al. [35] studied a dummy PV fitted with PCM enclosure with fins. Temperature drops from 87 °C to 37 °C and 87 °C to 35.3 °C have been reported with PCM- paraffin 32 and fin-enabled PCM respectively. Huang [36] has analysed the influence of two different phase change materials in same enclosure. It is found that the group of Paraffin wax 27- paraffin 21 works better. Emam et al. [37] reported the behaviour of phase change material enabled CPV as function of system's slope and established that non-zero slopes are always better than zero-slope. Cui et al. [38] obtained a decrease of 25% in temperature of PV while using CPV thermoelectric setup fitted with PCM – Sodium Hydroxide-Potassium Hydroxide. Method of separation of variables [39] can be used to obtain explicit equations [40] for temperature distributions [41] capturing the influence of inhomogeneous solar energy density [42].

After detailed study of the related works, it can be established that the PCM equipped with PV can elevate the power production. But, from the reported graphs, it also observed that the photovoltaic temperature starts rising quickly when PCM is completely liquefied. Thus, the optimization of PCM quantity needs to be carried out for proper electrical enhancement of PV. In the present study, the fins-fitted-PV-PCM has been optimized under different working circumstances for proper electrical enhancement. Setup has been modelled to incorporate the influence of working circumstances and the best deepness of fins-fitted-PCM enclosure has been computed for a range of wind pace, wind azimuth, surroundings temperature, melting point, successive fins distance, fins deepness, fins width and daily collective solar flux at PV surface in order to analyse the influence of working circumstances.

2. Physical model

The present work under consideration, as explained in Fig. 1, consists of two setups- PV-alone and PV fitted with a PCM enclosure having fins submerged in PCM. In both setups, PV is formed by placing 4 different coverings over a solid Tedlar platform. PCM's enclosure has the length and deepness of L and d_e respectively. w_f, d_f and d_{sf} are the fins width, fins deepness and successive fins distance respectively.

In order to capture the influence of working circumstances on the system performance, appropriate correlations for Nusselt number and heat transfer coefficient are presented. To model the PCM, a volume force term has been added along with the buoyancy force. Current study is relevant within the suppositions below

(i) Solar energy density is homogenous across the PV surface
(ii) All walls except front are perfectly insulated from outside causing adiabatic environment at respective walls
(iii) Respective traits of PV, PCM in solid phase, and PCM in liquid phase are homogenous across directions and space
(iv) Thermal resistance by films' interfaces is ignored.

3. Mathematical modelling

The thermal energy production in the PV is the solar flux absorbed by PV but not successful in power production. It is formulated as

$$E_{th} = \left[(\tau\alpha)_c \;\; S - \eta_{STC} S \left\{ 1 + \beta_c (T_{PV} - 25) + \gamma_c \ln\left(\frac{S}{1000}\right) \right\} \right] / t_{si} \tag{1}$$

The first part of the above equation is due to the absorbed flux and second is the power produced which incorporated the influence of temperature and solar flux. Some proportion of above thermal energy disperses from front of systems and rear of PV-alone system through radiation and convection. Forced component of convection is modelled incorporating the influence of pace (s_w) and azimuth (γ_w) of wind for front (h_f) and rear (h_r) [43]. Natural component of convection is modelled by using Nusselt number for front (Nu_f) and rear (Nu_r) [33,43].

The mathematics of the components of fins-fitted PV-PCM is discussed in following subsections.

3.1. Glass

The behaviour of the uppermost film in space and time can be estimated using solution to the equation below

$$\rho_{gl} C_{p,gl} \frac{\partial T_{gl}}{\partial t} = k_{gl} \left(\frac{\partial^2 T_{gl}}{\partial x^2} + \frac{\partial^2 T_{gl}}{\partial y^2} \right) \tag{2}$$

The solution can be obtained by putting the necessary boundary/initial conditions which are as follows [28]

$$k_{gl} \frac{\partial T_{gl}}{\partial y} = h_c [T_{gl} - T_a] + F_{gl\_sk} \sigma \varepsilon_{gl} [T_{gl}^4 - T_{sk}^4] + F_{gl\_gr} \sigma \varepsilon_{gl} [T_{gl}^4 - T_{gr}^4] \quad at \;\; glass \;\; top \tag{3}$$

$$k_{gl} \frac{\partial T_{gl}}{\partial x} = 0 \quad at \;\; edges \;\; of \;\; glass \tag{4}$$

$$k_{gl} \frac{\partial T_{gl}}{\partial y} = k_{EVA} \frac{\partial T_{EVA1}}{\partial y} \quad at \;\; glass - \;\; EVA \;\; interface \tag{5}$$

$$T_{gl} = T_a \;\; when \;\; t = 0 \tag{6}$$

Eq. (3) involves the thermal flow by convection from glass-film to the ambient, thermal flow by radiation from glass-film to the sky and from glass-film to ground. h_c must be estimated after considering both types of convection, viz. natural and forced.

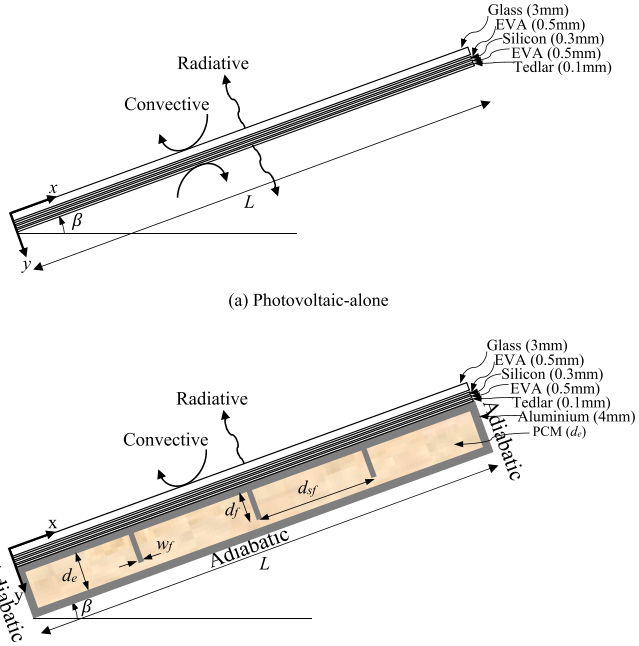

(a) Photovoltaic-alone

(b) fins fitted phase change material equipped photovoltaic

Fig. 1. Systems investigated under current work.

3.2. First film of Ethylene-Vinyl Acetate

The behaviour of the first film of Ethylene-Vinyl Acetate (EVA) in space and time can be estimated using solution to the equation below

$$\rho_{EVA} C_{p,EVA} \frac{\partial T_{EVA1}}{\partial t} = k_{EVA}\left(\frac{\partial^2 T_{EVA1}}{\partial x^2} + \frac{\partial^2 T_{EVA1}}{\partial y^2}\right) \tag{7}$$

The solution can be obtained by putting the necessary boundary/initial conditions which are as follows [28]

$$k_{EVA}\frac{\partial T_{EVA1}}{\partial x} = 0 \;\; at \;\; edges \;\; of \;\; EVA \tag{8}$$

$$k_{EVA}\frac{\partial T_{EVA1}}{\partial y} = k_{si}\frac{\partial T_{si}}{\partial y} \;\; at \;\; EVA - silicon \;\; interface \tag{9}$$

$$T_{EVA1} = T_a \;\; when \;\; t = 0 \tag{10}$$

3.3. Silicon film

The behaviour of the silicon film in space and time can be estimated using solution to the equation below

$$\rho_{si} C_{p,si} \frac{\partial T_{si}}{\partial t} = k_{si}\left(\frac{\partial^2 T_{si}}{\partial x^2} + \frac{\partial^2 T_{si}}{\partial y^2}\right) + E_{th} \tag{11}$$

The solution can be obtained by putting the necessary boundary/initial conditions which are as follows [28]

$$k_{si}\frac{\partial T_{si}}{\partial x} = 0 \;\; at \;\; edges \;\; of \;\; silicon \tag{12}$$

$$k_{si}\frac{\partial T_{si}}{\partial y} = k_{EVA}\frac{\partial T_{EVA2}}{\partial y} \;\; at \;\; silicon - EVA \;\; interface \tag{13}$$

$$T_{si} = T_a \;\; when \;\; t = 0 \tag{14}$$

3.4. Second film of Ethylene-Vinyl acetate

The behaviour of the second EVA film in space and time can be estimated using solution to the equation below

$$\rho_{EVA} C_{p,EVA} \frac{\partial T_{EVA2}}{\partial t} = k_{EVA}\left(\frac{\partial^2 T_{EVA2}}{\partial x^2} + \frac{\partial^2 T_{EVA2}}{\partial y^2}\right) \tag{15}$$

The solution can be obtained by putting the necessary boundary/initial conditions which are as follows [28]

$$k_{EVA}\frac{\partial T_{EVA2}}{\partial x} = 0 \;\; at \;\; edges \;\; of \;\; EVA \tag{16}$$

$$k_{EVA}\frac{\partial T_{EVA2}}{\partial y} = k_{te}\frac{\partial T_{te}}{\partial y} \;\; at \;\; EVA - tedlar \;\; interface \tag{17}$$

$$T_{EVA2} = T_a \;\; when \;\; t = 0 \tag{18}$$

3.5. Tedlar film

The behaviour of the tedlar film in space and time can be estimated using solution to the equation below

$$\rho_{te} C_{p,te} \frac{\partial T_{te}}{\partial t} = k_{te}\left(\frac{\partial^2 T_{te}}{\partial x^2} + \frac{\partial^2 T_{te}}{\partial y^2}\right) \tag{19}$$

The solution can be obtained by putting the necessary boundary/initial conditions which are as follows [28]

$$k_{te}\frac{\partial T_{te}}{\partial x} = 0 \;\; at \;\; edges \;\; of \;\; tedlar \tag{20}$$

$$k_{te}\frac{\partial T_{te}}{\partial y} = \begin{cases} h_c\,[T_{te} - T_a] + F_{te\_sk}\,\sigma\varepsilon_{te}\,[T_{te}^4 - T_{sk}^4] \\ \quad + F_{te\_gr}\,\sigma\varepsilon_{te}\,[T_{te}^4 - T_{gr}^4] \;\; at \;\; rear \;\; PValone \\ k_{al}\frac{\partial T_{al}}{\partial y} \quad at \;\; tedlar - aluminium \;\; interface \end{cases} \tag{21}$$

$$T_{te} = T_a \;\; when \;\; t = 0 \tag{22}$$

Eq. (21) involves the thermal flow by convection from tedlar-film to the ambient, thermal flow by radiation from tedlar-film to the sky and from tedlar-film to ground. h_c must be estimated after considering both types of convection, viz. natural and forced.

3.6. Fins fitted aluminium enclosure

The behaviour of the fins fitted enclosure in space and time can be estimated using solution to the equation below

$$\rho_{al} C_{p,al} \frac{\partial T_{al}}{\partial t} = k_{al}\left(\frac{\partial^2 T_{al}}{\partial x^2} + \frac{\partial^2 T_{al}}{\partial y^2}\right) \tag{23}$$

The solution can be obtained by putting the necessary boundary/initial conditions which are as follows [28]

$$k_{al}\frac{\partial T_{al}}{\partial x} = 0 \;\; at \;\; edges \;\; of \;\; aluminium \;\; box \tag{24}$$

$$k_{al}\frac{\partial T_{al}}{\partial y} = k_P\frac{\partial T_P}{\partial y} \;\; at \;\; aluminium - PCM \;\; interface \;\; along \;\; box \;\; length \tag{25}$$

$$k_{al}\frac{\partial T_{al}}{\partial x} = k_P\frac{\partial T_P}{\partial x} \;\; at \;\; aluminium - PCM \;\; interface \;\; along \;\; box \;\; depth \tag{26}$$

$$k_{al}\frac{\partial T_{al}}{\partial y} = 0 \;\; at \;\; rear \;\; of \;\; aluminium \;\; box \tag{27}$$

$$T_{al} = T_a \;\; when \;\; t = 0 \tag{28}$$

3.7. Phase change material

The behaviour of the phase change material in space and time can be estimated using solution to the equations below [28]

$$\rho_P C_P \frac{\partial T_P}{\partial t} = \nabla.\,(k_P \nabla T_P) - \frac{\partial}{\partial x}(\rho_P C_{p,P} u_x T_P) - \frac{\partial}{\partial y}(\rho_P C_{p,P} u_y T_P) \tag{29}$$

$$\rho_P\frac{\partial u_x}{\partial t} + \rho_P u_x\frac{\partial u_x}{\partial x} + \rho_P u_y\frac{\partial u_x}{\partial y} = -\frac{\partial p}{\partial x} + \mu_{P,l}\nabla^2\vec{u} + \rho_{P,l} g_x\,[1 - \beta_c(T_P - T_m)] - F_{ax} \tag{30}$$

$$\rho_P\frac{\partial u_y}{\partial t} + \rho_P u_x\frac{\partial u_y}{\partial x} + \rho_P u_y\frac{\partial u_y}{\partial y} = -\frac{\partial p}{\partial y} + \mu_{P,l}\nabla^2\vec{u} + \rho_{P,l} g_y\,[1 - \beta_c(T_P - T_m)] - F_{ay} \tag{31}$$

$$\nabla.\,\vec{u} = 0 \tag{32}$$

The solution can be obtained by putting the necessary boundary/initial conditions which are as follows [28]

$$k_P\frac{\partial T_P}{\partial y} = k_{al}\frac{\partial T_{al}}{\partial y} \;\; for \;\; aluminium - PCM \;\; interface \;\; along \;\; box \;\; length \tag{33}$$

$$k_P\frac{\partial T_P}{\partial x} = k_{al}\frac{\partial T_{al}}{\partial x} \;\; for \;\; aluminium - PCM \;\; interface \;\; along \;\; box \;\; depth \tag{34}$$

$$T_P = T_a \;\; when \;\; t = 0 \tag{35}$$

$$u_x = u_y = 0 \;\; for \;\; every \;\; inside \;\; surface \;\; of \;\; PCM \;\; box \tag{36}$$

$$u_x = u_y = 0 \quad when \quad t = 0 \tag{37}$$

The force F_a in Eqs. (30) and (31) is modelled as [21]

$$F_{ax} = \frac{-C\{1 - l(T)\}^2}{l(T)^3 + 10^{-3}} u_x \tag{38}$$

where l is the PCM's fraction in liquid state. C is Kozeny-Carman (permeability) constant [21] for which a very high value (10^5 kg/m^{3}s) is considered that helps F_a to become very large where PCM is in solid state (i.e $l = 0$) so that only solution to Eqs. (29)–(32) remains u = 0 m/s which vanishes the PCM speed inside the solid PCM. Most critical task at this juncture remains the modelling of PCM during its phase-change. It is a challenge in itself as the PCM experiences rapid property change while changing its phase. Appropriate model is presented so that the possibilities of non-convergence in this error-prone zone can be ruled out. Thus, a double-derivative differentiable function [21] has been adopted for *l(T)* which is the PCM's fraction in liquid state and is given as

$$l(T) = \sum_{i=0}^{6} a_i T^i \tag{39}$$

The coefficients can be obtained by putting the necessary boundary conditions which are as follows

$$l_{at \quad T_{P,s}} = 0,\ l_{at \quad T_m} = \frac{1}{2},\ l_{at \quad T_{P,l}} = 1 \tag{40}$$

$$\frac{dl}{dT}_{at \quad T_{P,s}} = \frac{d^2l}{dT^2}_{at \quad T_{P,s}} = \frac{dl}{dT}_{at \quad T_{P,l}} = \frac{d^2l}{dT^2}_{at \quad T_{P,l}} = 0 \tag{41}$$

The other thermal properties of phase change material as function of liquefied mass are modelled as [28]

$$C_p(T) = C_{p,s} + (C_{p,l} - C_{p,s})l(T) + H_f D(T) \tag{42}$$

$$\rho(T) = \rho_s + (\rho_l - \rho_s)l(T) \tag{43}$$

$$k(T) = k_s + (k_l - k_s)l(T) \tag{44}$$

4. Experimental Validation

Experiments to examine photovoltaic equipped phase change material's behaviour during heat transfer have been conducted [21]. The setup chosen for the purpose was a vertical aluminium enclosure filled by PCM- paraffin wax 25. The latent heat capacity of wax is 232 kJ/kg and the melting point is near to 26 °C. The enclosure's dimensions were 13.2 cm long and 2 cm deep. The PCM enclosure was fitted with aluminium sheets (0.4 cm thick) that are placed on rear as well as top. The setup was exposed to the environment with surroundings temperature as 293 K and solar energy density as 1 kW/m^2. The top and rear were left without insulation whereas all other sides of the enclosure were applied with the insulation. The temperature at enclosure's top was monitored as function of time.

In order to ascertain accuracy of the current work using experimental approach, the investigation has been done with identical variables. The interfaces are constructed by connecting the contact surfaces of individual layers of system using energy balance equations (Eqs. (5), (9), (13), (17), (21), (25) and (26)). Initially, each layer of system is set to ambient temperature using Eqs. ((6), (10), (14), (18), (22), (28), (35)) and the velocity of PCM is set to 0 m/s using Eq. (37). The exposure of solar energy density is set as heat generation using Eqs. (1) and (11). The insulated walls are equipped with no heat loss boundary condition using Eqs. ((4), (8), (12), (16), (20) and (24)). The non-insulated walls are equipped with proper convective and radiative heat losses to surroundings. The layer of PCM touching the aluminium container is set at zero velocity using Eq. (36). In order to satisfy the mass, momentum and energy balance in PCM, Eqs. (29)–(32) are used. The expansion of PCM upon heating is incorporated by the coefficient (β_c) appeared in Eqs. (30)–(31). In Fig. 2, the temperature pattern for enclosure's top is compared with the values reported from experiments.

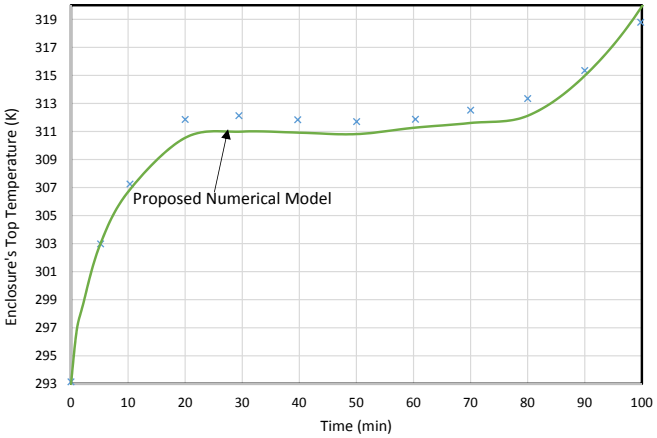

Fig. 2. Validation of proposed model with the reported experiments [21].

5. Results and discussion

The power production from the fins-fitted-PV-PCM have been computed for a range of wind pace, wind azimuth, surroundings temperature, PCM melting point, successive fins distance, fins deepness, fins width and deepness of fins-fitted-PCM enclosure. The best deepness of enclosure has been computed for proper electrical enhancement for a range of daily collective solar flux values. The system dimensions and the properties of phase change material are presented in Table 1.

5.1. Optimization of fins-fitted-phase change material enclosure

The power production from fins-fitted-PV-PCM is plotted in Fig. 3 for a range of deepness of enclosure. It is shown that, initially, the power production reduces quickly because the phase change material is completely solid and absorbs lesser heat from photovoltaic resulting in elevation of photovoltaic temperature and reduction in power production. After that, the power remains almost constant for long because the phase change material is now absorbing heat as heat of fusion which does not allow significant elevation in temperature resulting in constant temperature of photovoltaic. After that, the power production again

Table 1
Thermophysical properties of system and paraffin wax [28].

Property		Property	
$C_{p,al}$ (J/kgK)	903	T_m (K)	299
$C_{p,EVA}$ (J/kgK)	2090	t_{si} (mm)	0.3
$C_{p,gl}$ (J/kgK)	500	t_{te} (mm)	0.1
$C_{p,P,l}$ (J/kgK)	2400	L (m)	1
$C_{p,P,s}$ (J/kgK)	1800	$T_{P,s}$ (K)	298
$C_{p,si}$ (J/kgK)	677	$T_{P,l}$ (K)	300
$C_{p,te}$ (J/kgK)	1250	β (°)	45
H_f (J/kg)	232,000	β_c (K^{-1})	0.005
k_{al} (W/mK)	211	γ_c	0.085
k_{EVA} (W/mK)	0.35	ε_{gl}	0.85
k_{gl} (W/mK)	1.8	ε_{te}	0.91
$k_{P,l}$ (W/mK)	0.18	μ_l (kg/m-s)	0.0018
$k_{P,s}$ (W/mK)	0.19	ρ_{al} (kg/m^3)	2675
k_{si} (W/mK)	148	ρ_{EVA} (kg/m^3)	960
k_{te} (W/mK)	0.2	ρ_{gl} (kg/m^3)	3000
S (kW/m^2)	0.75	$\rho_{P,l}$ (kg/m^3)	749
s_w (m/s)	4	$\rho_{P,s}$ (kg/m^3)	785
T_a (K)	293	ρ_{si} (kg/m^3)	2330
t_{al} (mm)	4	ρ_{te} (kg/m^3)	1200
t_{EVA} (mm)	0.5	$(\tau\alpha)_c$	0.9
t_{gl} (mm)	3		

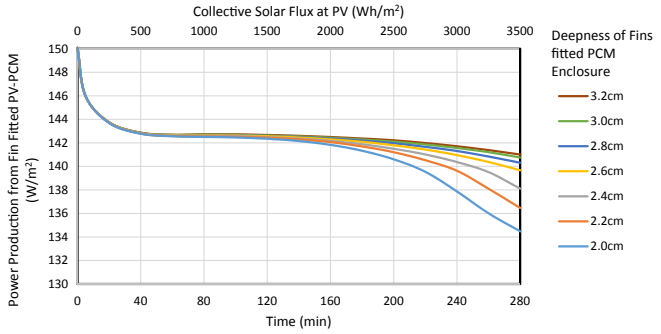

Fig. 3. Power production from fins fitted phase change material equipped photovoltaic for a range of deepness of enclosure.

reduces quickly because the phase change material is now almost liquefied resulting in lesser absorption of heat from PV and thus, quick elevation in photovoltaic temperature and reduction in power production.

It is also shown that the deeper fins-fitted-PCM enclosure is capable of increasing the period of power enhancement because of longer thermal regulation of photovoltaic. For a given collective daily solar flux at PV, there is no need to increase the deepness of enclosure beyond a limit. It is shown that, for daily collective solar flux at PV of 3000Wh/m^2, 2.8 cm deep enclosure is the best because by taking deeper enclosure than 2.8 cm, one cannot increase the power production by more than 1 W/m^2. Similarly, the optimum deepness has been calculated for different working circumstances following the process shown in Fig. 4.

5.2. Influence of wind pace

The best deepness of the fins-fitted-PCM enclosure is computed for a range of wind pace, fins dimensions and collective solar flux at PV and plotted in Fig. 5. For different successive fins distances (d_{sf}), it is shown that the change in wind pace from 0.2 m/s to 6 m/s results in reduction of the best deepness of enclosure from 5.2 cm to 3.7 cm, 5.6 cm to 4.0 cm, 5.8 cm to 4.2 cm, 5.9 cm to 4.3 cm and 5.9 cm to 4.3 cm for d_{sf} = 1 m, 1/2 m, 1/3 m, 1/4 m and 1/5 m respectively for daily

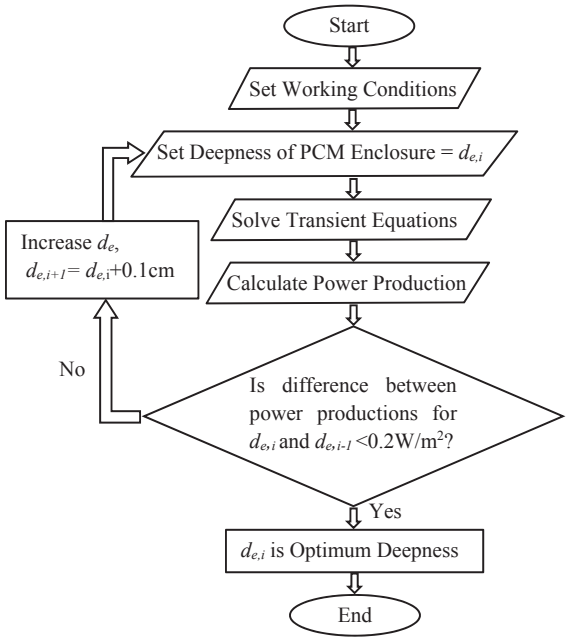

Fig. 4. Process followed to calculate optimum deepness of fins fitted phase change material enclosure.

collective solar flux at PV as 5000Wh/m^2 (Fig. 5a). It is because of the low wind pace reduces the heat loss which enhances the rate of heat absorption by phase change material and leads to early liquification (Fig. 6). Thus, low wind pace results in the requirement of deeper enclosure for proper electrical enhancement for whole duration. It is also shown that as distance of successive fins reduces, best deepness of enclosure increases (Fig. 5a). It is because of lesser distance enhances the rate of heat absorption by phase change material which results in early liquification and the requirement of deeper enclosure.

For different fins deepness (d_f) (Fig. 5b), it is shown that the change in wind pace from 0.2 m/s to 6 m/s results in reduction of the best deepness of enclosure from 5.4 cm to 3.9 cm, 5.5 cm to 4.0 cm and 5.9 cm to 4.3 cm for $d_f = d_e/3$, $2d_e/3$ and d_e respectively. Thus, deeper fin results in the requirement of deeper enclosure for proper electrical enhancement. It is also shown that there is a substantial raise in the best deepness of enclosure when fin deepness approaches d_e. It is because for fin deepness equals to enclosure deepness, heat gets directly transferred from front to rear through highly conductive fins and PCM is now

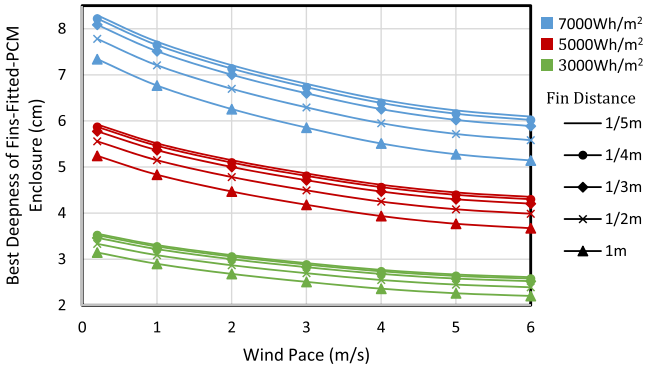

(a) Influence of Wind Pace for a range of Successive Fins Distance

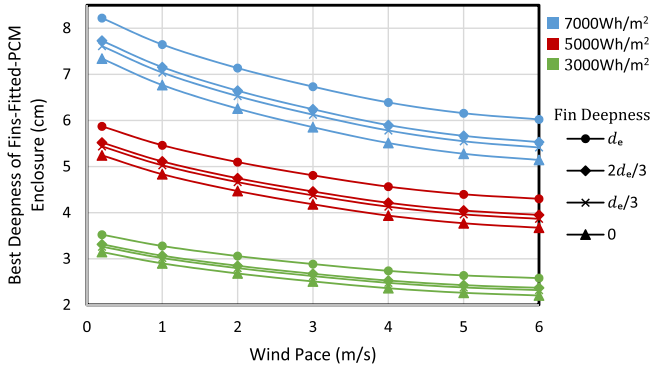

(b) Influence of Wind Pace for a range of Fin Deepness

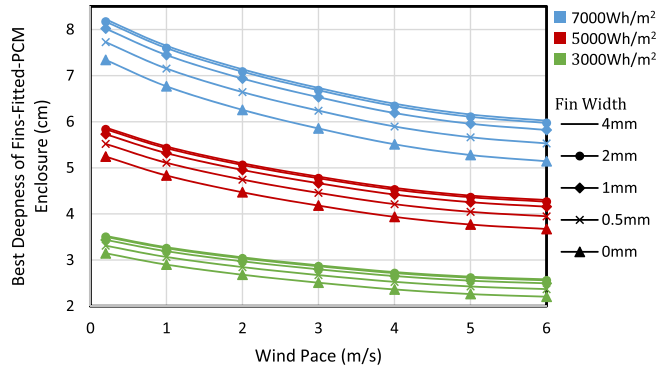

(c) Influence of Wind Pace for a range of Fin Width

Fig. 5. Best deepness of fins fitted phase change material enclosure for a range of wind pace, fins dimensions and daily collective solar flux at photovoltaic.

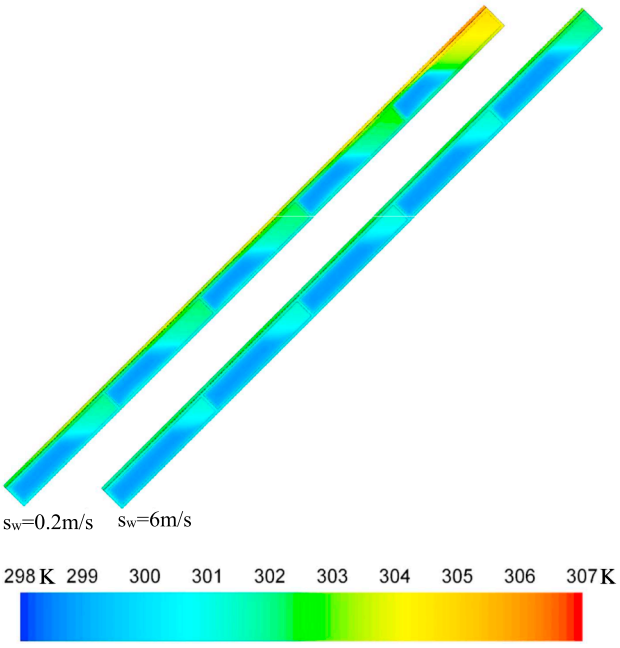

Fig. 6. Temperature contours (at t = 3 h) of the fins fitted phase change material equipped photovoltaic showing the higher speed of phase change material liquification for lesser wind pace.

absorbing heat from rear too resulting in quick liquification and requirement of deeper enclosure.

For different fins width (w_f) (Fig. 5c), it is shown that the change in wind pace from 0.2 m/s to 6 m/s results in reduction of the best deepness of enclosure from 5.4 cm to 4.0 cm, 5.7 cm to 4.2 cm, 5.9 cm to 4.3 cm and 5.9 cm to 4.3 cm for w_f = 0.5 mm, 1 mm, 2 mm and 4 mm respectively. It is also shown that as fin width increases, the best deepness of enclosure increases. It is because of enhanced rate of heat absorption by phase change material which results in early liquification and the requirement of deeper enclosure.

Thus, the results show that, for the climate with lesser wind pace (as compared to the climate with higher wind pace), larger quantity of phase change material is required to cool the PV and for proper electrical enhancement. It is because of the low wind pace reduces the heat loss from system which enhances the rate of heat absorption by phase change material. It results in early liquification of phase change material (Fig. 6) and leads to the requirement of larger quantity of phase change material for proper electrical enhancement.

5.3. Influence of wind azimuth

The best deepness of the fins-fitted-PCM enclosure is computed for a range of wind azimuths, fins dimensions and collective solar flux at PV and plotted in Fig. 7.

For different successive fins distances (d_{sf}), it is shown that the change in wind azimuth from 0° to 75° results in increment in the best deepness of enclosure from 3.9 cm to 4.8 cm, 4.3 cm to 5.2 cm, 4.5 cm to 5.4 cm, 4.6 cm to 5.5 cm and 4.6 cm to 5.5 cm for d_{sf} = 1 m, 1/2m, 1/3m, 1/4m and 1/5m respectively for daily collective solar flux at PV as 5000Wh/m^2 (Fig. 7a). It is because for the case of wind blowing normally with the PV, it removes the PV's heat effectively leaving lesser rate of heat absorption by phase change material. Thus, for the case of wind blowing across the PV, the rate of heat absorption by phase change material is higher and, thus, leads to early liquification (Fig. 8). Thus, high wind azimuths result in the requirement of deeper enclosure for proper electrical enhancement for whole duration.

For different fins deepness (d_f) (Fig. 7b), the change in wind azimuth from 0° to 75° results in increment in the best deepness of enclosure from 4.1 cm to 5.0 cm, 4.2 cm to 5.1 cm and 4.6 cm to 5.5 cm for $d_f = d_e/3$, $2d_e/3$ and d_e respectively.

For different fins width (w_f) (Fig. 7c), the change in wind azimuth from 0° to 75° results in increment in the best deepness of enclosure from 4.1 cm to 5.1 cm, 4.4 cm to 5.3 cm and 4.6 cm to 5.5 cm and 4.6 cm to 5.5 cm for w_f = 0.5 mm, 1 mm, 2 mm and 4 mm respectively.

Thus, the results show that, for the climate with lesser wind azimuth (as compared to the climate with higher wind azimuth), lesser quantity of phase change material is required to cool the PV and for proper electrical enhancement. It is because for the climate with wind blowing normally with the PV, it removes the PV's heat effectively leaving lesser rate of heat absorption by phase change material. It results in late liquification of phase change material (Fig. 8) and leads to the requirement of lesser quantity of phase change material for proper electrical enhancement.

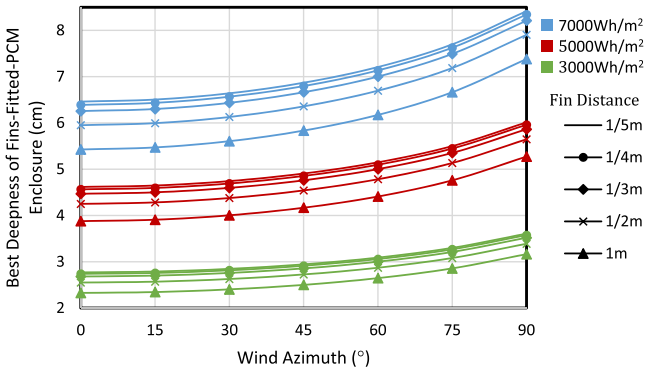

(a) Influence of Wind Azimuth for a range of Successive Fins Distance

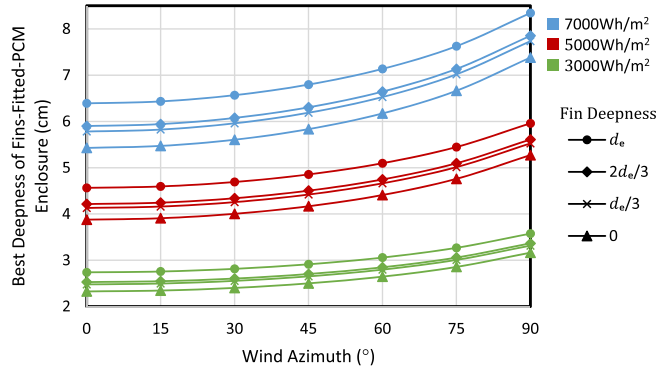

(b) Influence of Wind Azimuth for a range of Fin Deepness

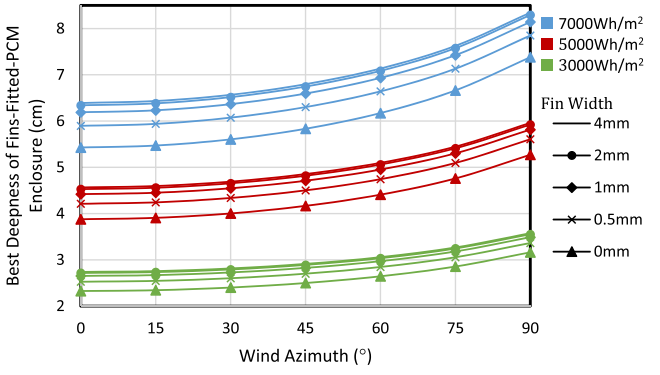

(c) Influence of Wind Azimuth for a range of Fin Width

Fig. 7. Best deepness of fins fitted phase change material enclosure for a range of wind azimuth, fins dimensions and daily collective solar flux at photovoltaic.

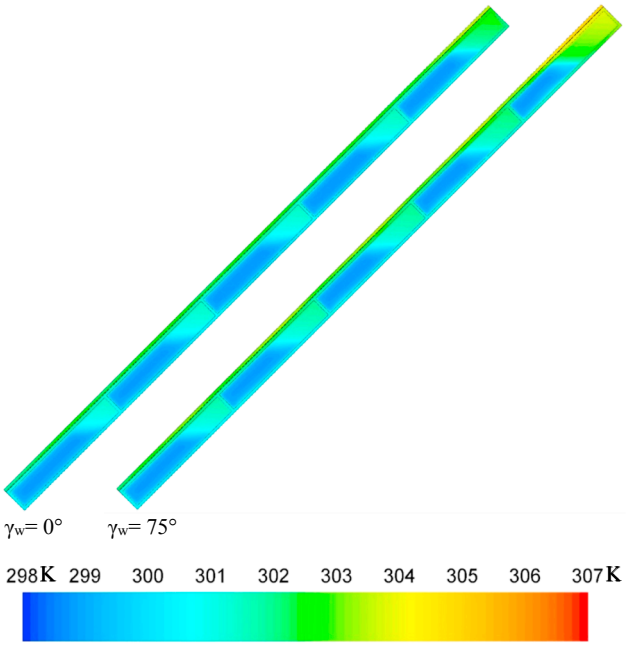

Fig. 8. Temperature contours (at t = 3 h) of the fins fitted phase change material equipped photovoltaic showing the higher speed of phase change material liquification for higher wind azimuth.

5.4. Influence of surroundings temperature

The best deepness of the fins-fitted-PCM enclosure is computed for a range of surroundings temperature, fins dimensions and collective solar flux at PV and plotted in Fig. 9. For different successive fins distances (d_{sf}), it is shown that the change in surroundings temperature from 289 K to 297 K results in increment in the best deepness of enclosure from 3.1 cm to 4.7 cm, 3.4 cm to 5.1 cm, 3.6 cm to 5.3 cm, 3.7 cm to 5.4 cm and 3.7 cm to 5.4 cm for d_{sf} = 1 m, 1/2 m, 1/3 m, 1/4 m and 1/5 m respectively for daily collective solar flux at PV as 5000Wh/m^2 (Fig. 9a). It is because the higher surroundings temperature causes heat absorption by phase change material (from PV) at higher pace resulting in early liquification and thus the requirement of deeper enclosure for proper electrical enhancement for whole duration.

For different fins deepness (d_f) (Fig. 9b), it is shown that the change in surroundings temperature from 289 K to 297 K results in increment in the best deepness of enclosure from 3.3 cm to 5.0 cm, 3.4 cm to 5.1 cm and 3.7 cm to 5.4 cm for $d_f = d_e/3$, $2d_e/3$ and d_e respectively.

For different fins width (w_f) (Fig. 9c), it is shown that the change in surroundings temperature from 289 K to 297 K results in increment in the best deepness of enclosure from 3.4 cm to 5.1 cm, 3.6 cm to 5.3 cm and 3.7 cm to 5.4 cm and 3.7 cm to 5.4 cm for w_f = 0.5 mm, 1 mm, 2 mm and 4 mm respectively.

Thus, the results show that, for the climate with higher ambient temperature (as compared to the climate with lesser ambient temperature), larger quantity of phase change material is required to cool the PV and for proper electrical enhancement. It is because the higher surroundings temperature causes heat absorption by phase change material (from PV) at higher pace. It results in early liquification of phase change material and leads to the requirement of larger quantity of phase change material for proper electrical enhancement.

5.5. Influence of melting point of phase change material

The best deepness of the fins-fitted-PCM enclosure is computed for a range of PCM melting points, fins dimensions and collective solar flux at PV and plotted in Fig. 10.

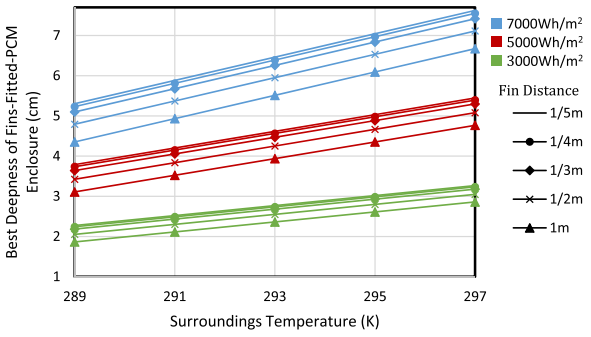

(a) Influence of Surroundings Temperature for a range of Successive Fins Distance

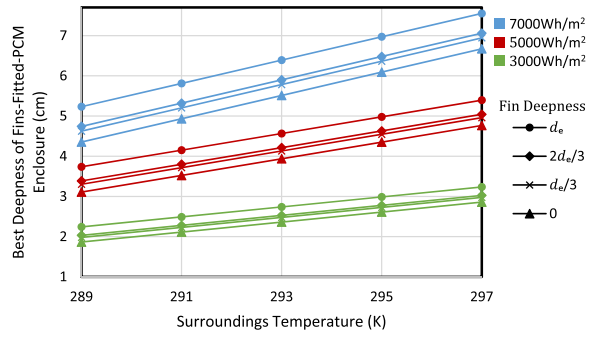

(b) Influence of Surroundings Temperature for a range of Fins Deepness

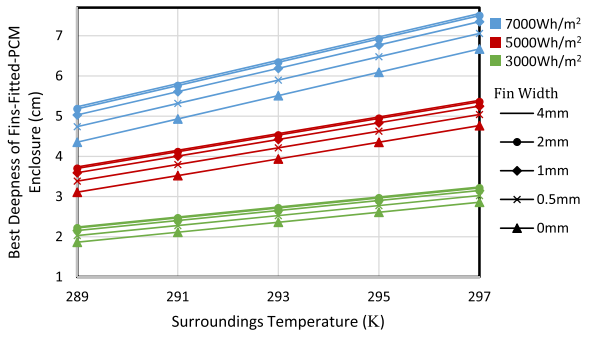

(c) Influence of Surroundings Temperature for a range of Fins Width

Fig. 9. Best deepness of fins fitted phase change material enclosure for a range of surroundings temperature, fins dimensions and daily collective solar flux at photovoltaic.

For different successive fins distances (d_{sf}), it is shown that the change in melting point from 295 K to 303 K results in reduction of the best deepness of enclosure from 4.9 cm to 3.0 cm, 5.2 cm to 3.3 cm, 5.4 cm to 3.5 cm, 5.5 cm to 3.6 cm and 5.5 cm to 3.6 cm for d_{sf} = 1 m, 1/2 m, 1/3 m, 1/4 m and 1/5 m respectively for daily collective solar flux at PV as 5000 Wh/m^2 (Fig. 10a). It is because the lesser melting point (close to surrounding temperature) keeps the photovoltaic at lesser temperature that reduces the thermal heat losses and enhances the rate of absorption by phase change material and, thus, leads to early liquification. Thus, lower melting point results in the requirement of deeper enclosure for proper electrical enhancement for whole duration.

For different fins deepness (d_f) (Fig. 10b), it is shown that the change in melting point from 295 K to 303 K results in reduction of the best deepness of enclosure from 5.0 cm to 3.2 cm, 5.1 cm to 3.3 cm and 5.5 cm to 3.6 cm for $d_f = d_e/3$, $2d_e/3$ and d_e respectively.

For different fins width (w_f) (Fig. 10c), it is shown that the change in melting point from 295 K to 303 K results in reduction of the best deepness of enclosure from 5.1 cm to 3.3 cm, 5.4 cm to 3.5 cm and 5.5 cm to 3.6 cm and 5.5 cm to 3.6 cm for w_f = 0.5 mm, 1 mm, 2 mm and 4 mm respectively.

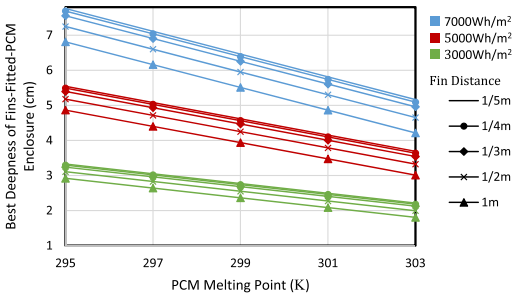

(a) Influence of Phase Change Material Melting Point for a range of Successive Fins Distance

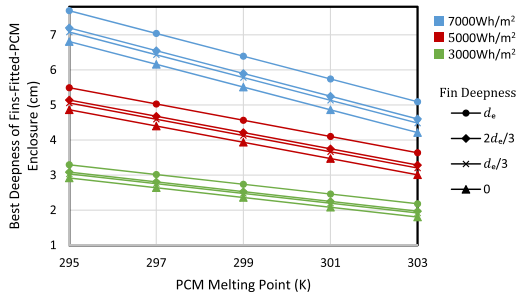

(b) Influence of Phase Change Material Melting Point for a range of Fin Deepness

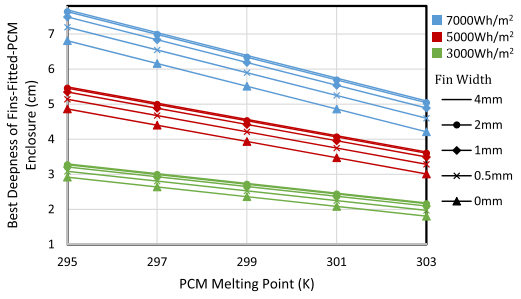

(c) Influence of Phase Change Material Melting Point for a range of Fin Width

Fig. 10. Best deepness of fins fitted phase change material enclosure for a range of melting point, fins dimensions and daily collective solar flux at photovoltaic.

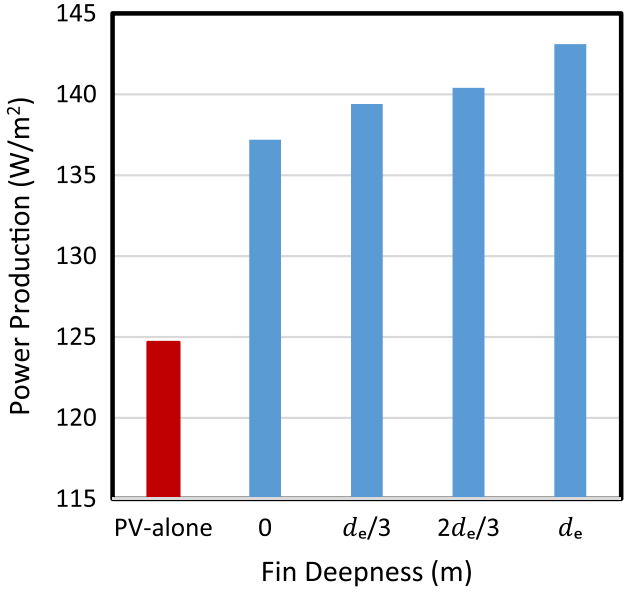

Fig. 11. Power production from photovoltaic-alone and fins fitted phase change material equipped photovoltaic for a range of fins deepness.

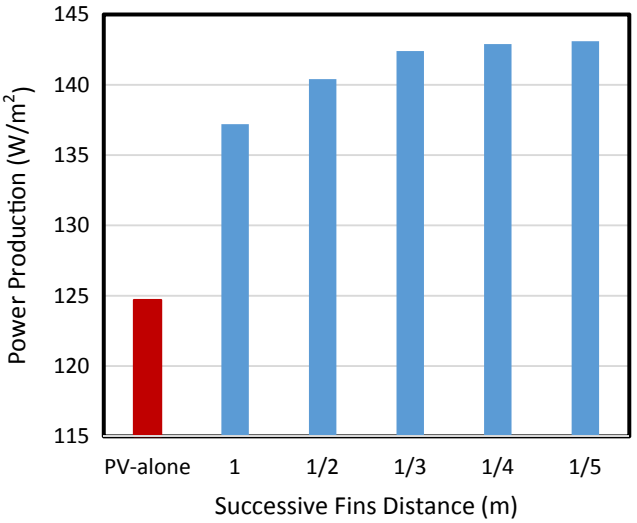

Fig. 12. Power production from photovoltaic-alone and fins fitted phase change material equipped photovoltaic for a range of fins successive distance.

5.6. Power production from photovoltaic-alone and fins fitted phase change material equipped photovoltaic

The power productions from PV-alone and fins-fitted-PV-PCM for a range of fins deepness (d_f) have been reported in Fig. 11. It is shown that the power production is elevated from 124.7 W/m^2 (for PV-alone) to 139.4 W/m^2, 140.4 W/m^2 and 143.1 W/m^2 by using fins deepness of $d_e/3$, $2d_e/3$ and d_e respectively. Thus, the results show that there is a substantial raise in the power production when fin deepness approaches d_e. It is because for fin deepness equals to enclosure deepness, heat gets directly transferred from front to rear through highly conductive fins and the rear gets heated up which enhances the heat removal from PV leading to decrease in PV temperature and increase in power production.

The power productions from PV-alone and fins-fitted-PV-PCM have been reported for a range of fins successive distance (d_{sf}) in Fig. 12. It is shown that the power production is elevated from 124.7 W/m^2 (for PV-alone) to 137.2 W/m^2, 140.4 W/m^2, 142.4 W/m^2, 142.9 W/m^2 and 143.1 W/m^2 by using fins successive distance of 1 m, 1/2m, 1/3m, 1/

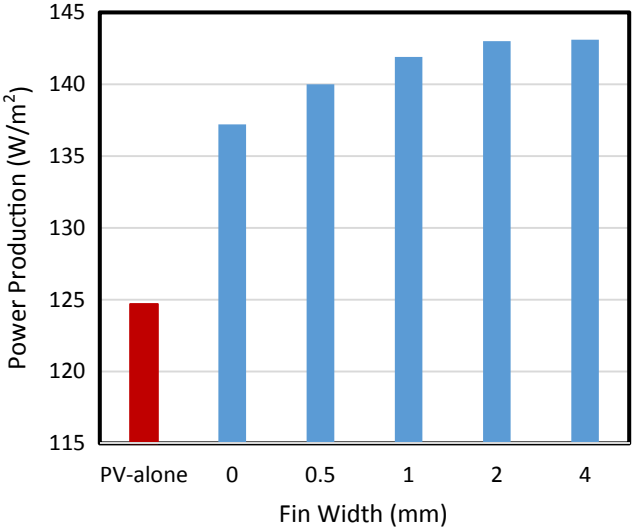

Fig. 13. Power production from photovoltaic-alone and fins fitted phase change material equipped photovoltaic for a range of fins widths.

4m and 1/5m respectively. Thus, the results show that as fins successive distance reduces, power production increases. It is because of lesser distance increases the number of fins which enhances the heat removal from PV leading to decrease in PV temperature and increase in power production.

The power productions from PV-alone and fins-fitted-PV-PCM have been reported for a range of fins width (w_f) in Fig. 13. It is shown that the power production is elevated from 124.7 W/m^2 (for PV-alone) to 140.0 W/m^2, 141.9 W/m^2, 143.0 W/m^2 and 143.1 W/m^2 by using fins width of 0.5 mm, 1 mm, 2 mm and 4 mm respectively. Thus, the results show that as fins width increases, power production increases. It is because with increase in fins width, the contact surface area of fins with PCM increases which enhances the heat removal from PV leading to decrease in PV temperature and increase in power production.

6. Conclusions

Fins-fitted-PV-PCM and PV-alone set-ups are modelled incorporating the influence of working circumstances. The best deepness of fins-fitted-PCM enclosure (d_e) has been computed for proper power enhancement for a range of daily collective solar flux at PV surface, wind pace, wind azimuth, surroundings temperature, melting point, successive fins distances (d_{sf}), fins deepness (d_f) and fins width (w_f). It is shown that

(i) The change in wind pace from 0.2 m/s to 6 m/s results in reduction of the best deepness of PCM enclosure from 5.2 cm to 3.7 cm, 5.6 cm to 4.0 cm, 5.8 cm to 4.2 cm, 5.9 cm to 4.3 cm and 5.9 cm to 4.3 cm for successive fins distance (d_{sf}) = 1 m, 1/2 m, 1/3 m, 1/4 m and 1/5 m respectively for daily collective solar flux at PV as 5000 Wh/m^2.
(ii) For different fins deepness, the change in wind pace from 0.2 m/s to 6 m/s results in reduction of the best deepness of enclosure from 5.4 cm to 3.9 cm, 5.5 cm to 4.0 cm and 5.9 cm to 4.3 cm for $d_f = d_e/3$, $2d_e/3$ and d_e respectively.
(iii) For different fins width, the change in wind pace from 0.2 m/s to 6 m/s results in reduction of the best deepness of enclosure from 5.4 cm to 4.0 cm, 5.7 cm to 4.2 cm, 5.9 cm to 4.3 cm and 5.9 cm to 4.3 cm for w_f = 0.5 mm, 1 mm, 2 mm and 4 mm respectively.
(iv) The power production is increased from 125 W/m^2 (for PV-alone) to 137 W/m^2, 140 W/m^2, 142 W/m^2, 143 W/m^2 and 143 W/m^2 with fins width of 0 mm, 0.5 mm, 1 mm, 2 mm and 4 mm respectively.

Minor error in the reported values of best deepness of PCM enclosure might exists due the fact that the present study does not incorporate the formation of crystals during cooling of PCM. It can reduce the flow of heat through the PCM which leads to late liquification of PCM. Thus, the required deepness of PCM enclosure is marginally lesser than the reported one. The other error lies in the fact that the present study assumes ideal connection of PCM enclosure with that of PV rear. In reality, the non-ideal connection reduces the flow of heat (to some extent) from PV to PCM enclosure which leads to late liquification of PCM. Thus, the required deepness of PCM enclosure is marginally lesser than the reported one.

Acknowledgment

Dr. Sourav Khanna, Prof. K.S. Reddy and Prof. Tapas K. Mallick gratefully acknowledge the financial support from EPSRC-DST funded Reliable and Efficient System for Community Energy Solution - RESCUES project (EP/K03619X/1) and UKIERI-DST2016-17-0089 project. In support of open access research, all underlying article materials (such as data, samples or models) can be accessed upon request via email to the corresponding author.

References

[1] Baygi SRM, Sadrameli SM. Thermal management of photovoltaic solar cells using polyethylene glycol 1000 (PEG1000) as a phase change material. Therm Sci Eng Progr 2018;5:405–11.
[2] Huang MJ, Eames PC, Norton B. Phase change materials for limiting temperature rise in building integrated photovoltaics. Solar Energy 2006;80:1121–30.
[3] Huang MJ, Eames PC, Norton B. Comparison of predictions made using a new 3D phase change material thermal control model with experimental measurements and predictions made using a validated 2D model. Heat Transf Eng 2007;28:31–7.
[4] Hasan A, McCormack SJ, Huang MJ, Sarwar J, Norton B. Increased photovoltaic performance through temperature regulation by phase change materials: materials comparison in different climates. Sol Energy 2015;115:264–76.
[5] Indartono YS, Suwono A, Pratama FY. Improving photovoltaics performance by using yellow petroleum jelly as phase change material. Int J Low-Carbon Technol 2014:1–5.
[6] Hasan A, McCormack SJ, Huang MJ, Norton B. Evaluation of phase change materials for thermal regulation enhancement of building integrated photovoltaics. Solar Energy 2010;84:1601–12.
[7] Kamkari B, Groulx D. Exp Therm Fluid Sci 2018;97:94–108.
[8] Sharma S, Tahir A, Reddy KS, Mallick TK. Performance enhancement of a building integrated concentrating photovoltaic system using phase change material. Sol Energy Mater Sol Cells 2016;149:29–39.
[9] Sharma S, Micheli L, Chang WA, Tahir KS Reddy, Mallick TK. Appl Energy 2017;208:719–33.
[10] Preet S, Bhushan B, Mahajan T. Experimental investigation of water based photovoltaic/thermal (PV/T) system with and without phase change material (PCM). Solar Energy 2017;155:1104–20.
[11] Browne MC, Norton B, McCormack SJ. Sol Energy 2016;133:533–48.
[12] Browne MC, Quigley D, Hard HR, Gilligan S, Ribeiro NCC, Almeida N, et al. Energy Procedia 2016;91:113–21.
[13] Browne MC, Lawlor K, Kelly A, Norton B, McCormack SJ. Indoor characterisation of a photovoltaic/thermal phase change material system. Energy Proc 2015;70:163–71.
[14] Su Y, Zhang Y, Shu L. Sol Energy 2018;159:777–85.
[15] Al Siyabi I, Khanna S, Mallick T, Sundaram S. Multiple Phase Change Material (PCM) configuration for PCM based heat sinks—an experimental study. Energies 2018;11(7):1629.
[16] Al Siyabi I, Khanna S, Mallick T, Sundaram S. Electricity enhancement and thermal energy production from concentrated photovoltaic integrated with a 3-layered stacked micro-channel heat sink. AIP Conference Proceedings 2018 2012. p. 080001. https://doi.org/10.1063/1.5053529.
[17] Brano VL, Ciulla G, Piacentino A, Cardona F. Renew Energy 2014;68:181–93.
[18] Ciulla G, Brano VL, Cellura M, Franzitta V, Milone D. Energy Procedia 2012;30:198–206.
[19] Atkin P, Farid MM. Improving the efficiency of photovoltaic cells using PCM infused graphite and aluminium fins. Sol Energy 2015;114:217–28.
[20] Kibria MA, Saidur R, Al-Sulaiman FA, Aziz MMA. Development of a thermal model for a hybrid photovoltaic module and phase change materials storage integrated in buildings. Sol Energy 2016;124:114–23.
[21] Biwole PH, Eclache P, Kuznik F. Phase-change materials to improve solar panel's performance. Energy Build 2013;62:59–67.
[22] Biwole PH, Groulx D, Souayfane F, Chiu T. Influence of fin size and distribution on solid-liquid phase change in a rectangular enclosure. Int J Therm Sci 2018;124:433–46.
[23] Groulx D, Biwole PH. Solar PV passive temperature control using phase change materials. 15th International Heat Transfer Conference, August 10–15, 2014, 2014, Kyoto; Japan. 2014.
[24] Kant K, Shukla A, Sharma A, Biwole PH. Heat transfer studies of photovoltaic panel coupled with phase change material. Sol Energy 2016;140:151–61.
[25] Park J, Kim T, Leigh SB. Application of a phase-change material to improve the electrical performance of vertical-building-added photovoltaics considering the annual weather conditions. Sol Energy 2014;105:561–674.
[26] Su D, Jia Y, Alva G, Liu L, Fang G. Comparative analyses on dynamic performances of photovoltaic–thermal solar collectors integrated with phase change materials. Energy Convers Manage 2017;131:79–89.
[27] Khanna S, Reddy KS, Mallick TK. Climatic behaviour of solar photovoltaic integrated with phase change material. Energy Conversion Manage 2018;166:590–601.
[28] Khanna S, Reddy KS, Mallick TK. Effect of climate on electrical performance of finned phase change material integrated solar photovoltaic. Solar Energy 2018;174:593–605.
[29] Khanna S, Reddy KS, Mallick TK. Optimization of finned solar photovoltaic phase change material (Finned PV PCM) system. Int J Therm Sci 2018;130:313–22.
[30] Khanna S, Reddy KS, Mallick TK. Optimization of solar photovoltaic system integrated with phase change material. Solar Energy 2018;163:591–9.
[31] Khanna S, Reddy KS, Mallick TK. Performance analysis of tilted photovoltaic system integrated with phase change material under varying operating conditions. Energy 2017;133:887–99.
[32] Khanna S, Reddy KS, Mallick TK. Photovoltaic system integrated with phase change material for South West UK climate. AIP Conference Proceedings 2018 2012. p. 080007. https://doi.org/10.1063/1.5053535.
[33] Khanna S, Sundaram S, Reddy KS, Mallick TK. Performance analysis of perovskite and dye-sensitized solar cells under varying operating conditions and comparison with monocrystalline silicon cell. Appl Therm Eng 2017;127:559–65.

[34] Emam M, Ahmed A. Cooling concentrator photovoltaic systems using various configurations of phase-change material heat sinks. Energy Conversion Manage 2018;158:298–314.
[35] Huang MJ, Eames PC, Norton B. Int J Heat Mass Transf 2004;47:2715–33.
[36] Huang MJ. Sol Energy Mater Sol Cells 2011;95:957–63.
[37] Emam M, Ookawara S, Ahmed M. Sol Energy 2017;150:229–45.
[38] Cui T, Xuan Y, Li Q. Energy Convers Manage 2016;112:49–60.
[39] Khanna S, Sharma V, Singh S, Kedare SB. Explicit expression for temperature distribution of receiver of parabolic trough concentrator considering bimetallic absorber tube. Appl Therm Eng 2016;103:323–32.
[40] Khanna S, Sharma V. Explicit analytical expression for solar flux distribution on an undeflected absorber tube of parabolic trough concentrator considering sun-shape and optical errors. J Solar Energy Eng 2016;138(1):011010. https://doi.org/10.1115/1.4032122.
[41] Khanna S, Sharma V. Effect of number of supports on the bending of absorber tube of parabolic trough concentrator. Energy 2015;93:1788–803.
[42] Sharma V, Khanna S, Nayak JK, Kedare SB. Effects of shading and blocking in compact linear Fresnel reflector field. Energy 2016;94:633–53.
[43] Kaplani E, Kaplanis S. Thermal modelling and experimental assessment of the dependence of PV module temperature on wind velocity and direction, module orientation and inclination. Sol Energy 2014;107:443–60.